Polymer Composites

WILEY | spe INSPIRING PLASTICS PROFESSIONALS

RESEARCH ARTICLE OPEN ACCESS

Thermal Management and Mechanical Properties of Epoxy-Sandwich Composites Containing Microencapsulated Phase Change Material

Laura Simonini[1,2] | Silvia Santagiuliana[1] | Alessandro Tomasini[1] | Giulia Fredi[1,2] | Alessandro Pegoretti[1,2]

[1]Department of Industrial Engineering, University of Trento, Trento, Italy | [2]National Interuniversity Consortium of Materials Science and Technology (INSTM), Florence, Italy

Correspondence: Laura Simonini (laura.simonini@unitn.it)

Received: 25 November 2025 | **Revised:** 12 January 2026 | **Accepted:** 10 February 2026

Keywords: epoxy foam | mechanical testing | PCM | sandwich | thermal management

ABSTRACT

In this work, epoxy (EP) foams containing 10, 20, and 30 wt% of microencapsulated phase change materials (PCMs) were developed as potential cores for multifunctional sandwich composites combining structural performance with latent heat storage capability. The foams were characterized for their microstructural, thermal and mechanical properties. Microstructural analysis revealed that PCMs dispersed within the cell walls and promoted an increase of open porosity. Despite these morphological changes, heat flow meter analysis confirmed that the foams retained enough insulating properties. Differential scanning calorimetry showed a melting enthalpy up to 36 J/g for a 30 wt% PCM content. Infrared thermography revealed a delay in their surface temperature during heating and cooling cycles, especially for a PCM content equal to or higher than 20 wt%. Flexural and compressive properties of the foams decreased with PCMs, regardless of the testing temperature. The foams were then used as core in sandwich composites. Mechanical tests showed improvements in core shear flexural strength (+37%), facing stress (+47%), and edgewise compression strength (+20%) at 20 wt% PCM. Therefore, 20 wt% PCM was found to be the most promising concentration for balancing the mechanical performance and the thermal buffering of multifunctional composites. The developed composites could have applications in aerospace, automotive, and refrigerated transportation industries.

1 | Introduction

Sandwich composites are made of two rigid skins bonded to a lightweight core and they represent a well-established method to achieve high specific stiffness and strength with a minimal weight. Sandwiches are widely used in transportation [1], aerospace [2], marine [3], and civil engineering [4] applications. In addition, sandwiches are also attractive due to the flexibility in core selection, which allows balancing stiffness, strength, energy absorption, and thermal behavior [5]. Example of core materials are (i) polymer foams [6], which are frequently preferred due to their versatility and easy fabrication, (ii) honeycomb structures [7], which are effective in terms of in-plane strength and stiffness, and (iii) balsa wood architectures [8], which offers a natural, affordable solution. Among the polymeric cores, epoxy foams are gaining significant attention [9, 10]. Compared to the commonly used polyurethane or polystyrene foams, epoxy foams offer superior thermal stability and chemical resistance, as well as excellent adhesion to fiber-reinforced skins [11]. They can be utilized in applications where both thermal durability and structural performance are required due to their relatively high glass transition temperature and dimensional stability under load [12].

Highlights

- PCMs were incorporated into EP foams and used as cores for sandwich composites.
- PCMs provided heat storage capability to the EP foams.
- Sandwich composites exhibited good flexural and compressive properties.
- PCMs at 20 wt% provided the balance between thermal and mechanical performance.

In addition to mechanical efficiency, sandwich composites can also offer additional functionalities [13, 14]. One in particular is thermal management, since many modern systems need accurate temperature control to guarantee energy efficiency, safety and product preservation [15]. Traditional strategies to achieve thermal insulation in cores have focused on the reduction of thermal conductivity, which slows down the heat flow under steady-state conditions [16]. However, this approach is less effective when dealing with variable or transient heat sources [17]. In such cases, it can be advantageous to provide thermal inertia, that is, the delay and buffering of the material's response to temperature changes [18]. This can be achieved by the introduction of phase change materials (PCMs) into the core structure [19]. In fact, PCMs can absorb and release large amounts of latent heat during melting and solidification [20]. Organic PCMs, such as paraffins and fatty acids, are particularly used in the low-medium temperature range (0°C–100°C) due to their suitable transition temperatures, high enthalpy of fusion, non-toxicity and chemical stability [21]. Moreover, microencapsulation enables their safe and practical incorporation into polymer matrices by preventing leakage during phase transition and allowing them to act as solid fillers [22, 23]. Consequently, PCM-filled polymers have been extensively studied for their potential applications in heat storage and temperature regulation of buildings, packaging, and electronics [24–26]. However, while most research on PCM-filled rigid foams has focused on polyurethane matrices [27], the use of epoxy foams as a host material is rather underexplored. In the literature, no reports on epoxy foams containing PCM can be found with the only exception of epoxy/hollow glass microsphere (HGM) syntactic foams [28–30]. At the same time, research has been largely focused on the heat storage and management properties of composites, with a limited attention to the mechanical performance of PCM containing foams and relative sandwiches for structural applications [31].

Therefore, this work aims at investigating the use of epoxy foams filled with different amounts of PCMs (10, 20, 30 wt%) as potential cores for multifunctional sandwich composites. The foams were first characterized for their microstructural, thermal, and mechanical properties, then they were incorporated as cores in sandwich composites with carbon/epoxy laminate skins. The resulting sandwiches were tested under flexural and edgewise compression loading to provide information on failure modes and skin/core adhesion. Therefore, the proposed approach demonstrated the potential of such lightweight composites to meet both structural and thermal requirements, simultaneously.

2 | Experimental Part

2.1 | Materials

Epoxy base PB170 (viscosity at 20°C = 15,000 mPa·s and density at 20°C = 1.12 g/cm^3) and hardener DM02 (viscosity at 20°C = 130 mPa·s and density at 20°C = 0.98 g/cm^3) were provided by Elantas Italia Srl (Colecchio, Italy) and used for the preparation of the sandwich cores. Base and hardener were mixed at a ratio of 100:36 by weight, as described in their datasheet. MPCM 32D microencapsulated phase change materials were supplied by Microtek Laboratories Inc. (OH, USA) in the form of dry powder with a mean particle size of 15–30 μm, a density of 0.90 g/cm^3, a nominal melting point of 32°C ± 2°C and a latent heat of fusion of 160 J/g. The material is paraffin wax contained in melamine-formaldehyde microcapsules.

Epoxy base Elan-tech EC 157 (viscosity at 25°C = 700 mPa·s and density at 25°C = 1.15 g/cm^3) and the hardener Elan-tech W 342 (viscosity at 25°C = 50 mPa·s and density at 25°C = 0.95 g/cm^3) were provided by Elantas Italia Srl (Colecchio, Italy) and used for the preparation of the sandwich skins. Base and hardener were mixed at a ratio of 100:30 by weight, as described in their datasheets.

Unidirectional plain carbon fabric GV 201 (mass per unit area = 217 g/cm^3) was provided by G. Angeloni Srl (Venezia, Italy).

2.2 | Sample Preparation

2.2.1 | Preparation of Foam Samples

The stages of the preparation process are illustrated in Figure 1a–d. The epoxy base (PB170) and the hardener (DM02) were weighed and poured into separate beakers. The required amount of PCMs was weighed and distributed equally between the two beakers and mechanically mixed at 50 rpm for 1 min. Once the mixtures were homogeneous, (a) the contents of the two beakers were combined, (b) mechanically mixed with the same parameters, and then (c) poured into a 250 × 250 × 22 mm^3 mold lined internally with polytetrafluoroethylene (PTFE), to allow the foam to be easily removed. The mixture in the mold was left at room temperature for 24 h to foam and reach the maximum thickness. The curing process was performed in an oven at 40°C for 6 h followed by a second heat treatment at 60°C for 16 h. After curing, (d) the foams were demolded and milled on both surfaces to remove the thin, denser outer layer formed during foaming, thus obtaining panels with final dimensions of 200 × 200 × 20 mm^3. The prepared foams are summarized in Table 1, where the nominal weight compositions are specified.

2.2.2 | Preparation of Sandwich Composites

After foam characterization, panels were used as cores for sandwiches. The composite skins were applied on cores using a combination of hand lay-up and vacuum bagging techniques. First, three carbon fiber fabrics were laid on a flat metal plate and impregnated with the resin system consisting of epoxy base EC

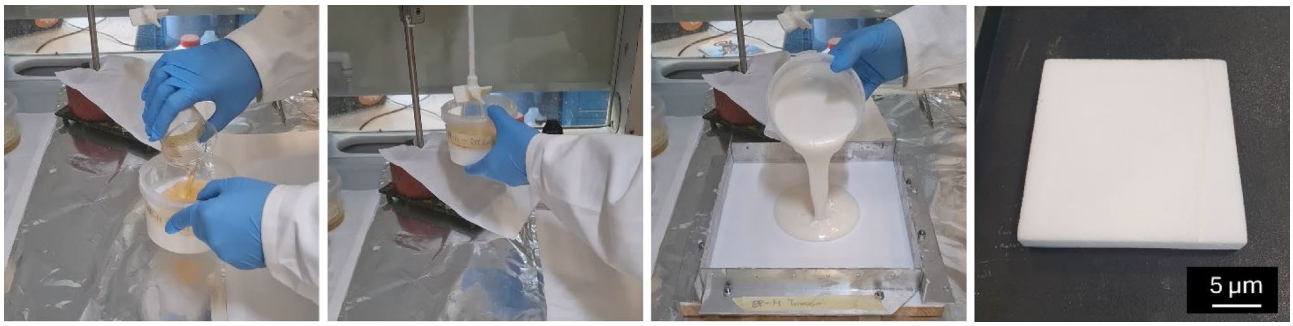

FIGURE 1 | Schematic illustration of the foam preparation process: (a) addition of epoxy resin, curing agent and PCMs into a beaker, (b) mechanical mixing, (c) casting of the reactive mixture into a mold and (d) aspect of the foam obtained after curing and milling.

157 and hardener W 342. The foam panel was subsequently impregnated on both sides with the same resin mixture to enhance skin/core interfacial adhesion before being placed on top of the three layers of carbon fiber. Another three carbon fiber fabrics, impregnated with the same resin system, were then plied on top of the foam, completing the sandwich structure. The entire assembly was sealed using a vacuum bag on the metal plate with sealant tape, and vacuum was applied to ensure proper compaction and resin distribution. The composite structure was cured at room temperature for 24 h, demolded, and post-cured at 60°C for 15 h. The prepared sandwiches are summarized in Table 1, where the type of core and skin used are specified.

2.3 | Experimental Techniques

2.3.1 | Characterization of the Foam Samples

2.3.1.1 | **Microstructural Characterization.** The morphology of the foam samples was investigated using a Zeiss Supra 40 field-emission scanning electron microscope (FESEM) (Carl Zeiss AG, Oberkochen, Germany). Foam samples measuring $20 \times 10 \times 10\,mm^3$ were immersed in liquid nitrogen for 1 h, then extracted and broken in half to reveal a brittle fracture surface. The obtained surfaces were coated with a layer of a platinum/palladium (Pt/Pd) alloy (80:20) for 20 s with a thickness of about 5 nm. From the micrographs, the diameter of approximately 100 cells per composition was measured using ImageJ software (version 1.53a).

The porosity of the foams was evaluated through the calculation of the geometrical and the theoretical density of the samples. The geometrical density (ρ_{bulk}) is defined as the experimental density of a structure that includes defects and porosity, and it was calculated according to Equation (1):

$$\rho_{bulk} = \frac{m_{sample}}{V_{bulk}}, \tag{1}$$

where m_{sample} is the weight (in g) and V_{bulk} is the geometrical volume (in cm^3) of rectangular samples, having dimensions $90 \times 20 \times 10\,mm^3$, cut from the prepared foams. At least five specimens were measured for each composition. Masses were measured with an analytical balance ($d = 0.0001$ g) and lengths with a caliper ($d = 0.01$ mm).

TABLE 1 | List of prepared samples with nominal weight compositions.

Foam samples	Epoxy (PB170 + DM02) (wt%)	PCM (wt%)
EP	100	0
EP-10	90	10
EP-20	80	20
EP-30	70	30
Sandwich samples	**Core**	**Skin**
s-EP	EP	Epoxy (EC157 + W342)/ carbon laminate
s-EP-10	EP-10	Epoxy (EC157 + W342)/ carbon laminate
s-EP-20	EP-20	Epoxy (EC157 + W342)/ carbon laminate
s-EP-30	EP-30	Epoxy (EC157 + W342)/ carbon laminate

The theoretical density (ρ_{th}) is defined as the density of the solid material composing the foam (epoxy resin and PCM microcapsules), calculated using the rule of mixtures from the densities and weight fractions of epoxy resin and PCM, as described in Equation (2):

$$\rho_{th} = \frac{1}{\sum_i \frac{W_i}{\rho_i}} = \frac{1}{\frac{W_{base}}{\rho_{base}} + \frac{W_{hard}}{\rho_{hard}} + \frac{W_{PCM}}{\rho_{PCM}}}, \tag{2}$$

where W_i and ρ_i are the weight fraction and the density (from datasheets) of each constituent (i.e., epoxy base, hardener, and PCMs). This method assumes that the final density of the foam walls are the weighted average of the densities of the base and hardener in their uncured form, which is not completely accurate. However, this is the only method to calculate the theoretical density of the unfoamed epoxy, which is needed to determine the total, open, and closed porosity of the developed foams. Indeed, it is not possible, with the employed epoxy system, to produce an unfoamed sample.

Finally, the apparent density (ρ_{app}) is defined as the experimental density of a structure that includes closed pores and internal defects but excludes the contribution of the open pores. It was measured with an AccuPyc 1330 helium pycnometer (Micromeritics Instrument Corporation, Norcross, GA, USA) following ASTM D6226 standard. Measurements were conducted at 23°C using a 1 cm^3 cell and performing 99 measurements for each sample.

Hence, the total porosity (P_{tot}) of the prepared foams was calculated as reported in Equation (3),

$$P_{tot} = 1 - \frac{\rho_{bulk}}{\rho_{th}}, \tag{3}$$

and the open porosity (P_{open}) was calculated as reported in Equation (4),

$$P_{open} = 1 - \frac{\rho_{bulk}}{\rho_{app}}, \tag{4}$$

Therefore, the closed porosity (P_{closed}) was calculated as shown in Equation (5),

$$P_{closed} = P_{tot} - P_{open}, \tag{5}$$

2.3.1.2 | Thermal Characterization. Thermogravimetric analysis on the foam samples was conducted by using a Mettler TG50 thermobalance (Mettler Toledo, Columbus, OH, USA) under a nitrogen flow of 100 mL/min, and imposing a heating ramp from 30°C to 700°C and a heating rate of 10°C/min. The residual mass at 700°C (m_{700}), the temperature of the degradation at 5% of mass loss ($T_{5\%}$), and the temperature of maximum degradation rate (T_{max}), obtained from the peak of the derivative of TGA thermogram (DTG), were assessed. One specimen was tested for each composition.

Differential scanning calorimetry (DSC) was performed via a Mettler DSC 30 (Mettler Toledo Inc., Columbus, Ohio, USA). Specimens were subjected to a heating/cooling/heating cycle between −40°C and 150°C at ±10°C/min, under a constant nitrogen flow of 100 mL/min. The tests allowed measuring the melting and crystallization temperatures (T_m and T_c) and enthalpies (ΔH_m and ΔH_c) of the PCM contained in the foams.

The thermal conductivity (λ) of the prepared foams was determined on specimens of nominal dimension of 200 × 200 × 15 mm^3 using a Netzsch HFM 446 Small Lambda instrument (NETZSCH-Gerätebau, Selb, Germany) at constant temperatures of 10°C, 30°C, and 50°C (i.e., below, in the proximity, and above the melting temperature of the PCM, 32°C) and according to ASTM C518-21. Three specimens were tested for each composition.

The thermal diffusivity (α) of the foams was measured at 20°C using laser flash analysis (LFA) with a Netzsch LFA 447 instrument (Netzsch Gerätebau GmbH, Selb, Germany). One circular specimen with a diameter of 12.7 mm and a thickness of 3 mm was tested for each composition.

The thermal behavior of the foams was also analyzed with the FLIR E6 IR thermal imaging camera (Teledyne FLIR llc, NH, USA), to evaluate how the PCMs influenced the heating and cooling rates of the foams. For the experiment under heating conditions, the specimens were conditioned at −18°C for at least 12 h and then placed in an oven at 50°C and left heating while the surface temperature was recorded with the thermal camera. For the experiment under cooling conditions, the specimens were conditioned at 70°C for at least 12 h and then placed at 10°C and left cooling while the surface temperature was recorded with the thermal camera. The test was performed on one specimen per composition, with nominal dimensions 150 × 150 × 20 mm^3. The emissivity of the material was set to 0.96.

2.3.1.3 | Mechanical Characterization. Three-point flexural tests were performed using an Instron 4502 machine (Instron Mechanical Testing Systems, Norwood, MA, USA), equipped with a load cell of 10 kN, to determine the specific values (i.e., divided by the geometrical density) of flexural modulus (E_f) and strength (σ_f) according to ISO 1209-2. Samples had nominal dimensions of 200 × 20 × 15 mm^3, and a span-to-depth ratio of 12 was used. The tests were carried out at 20°C and 40°C, at a crosshead speed of 20 mm/min. At least 10 specimens for each composition were tested.

Quasi-static compression tests were performed with the Instron 4502 machine (Instron Mechanical Testing Systems, Norwood, MA, USA), equipped with a load cell of 10 kN, to determine the compressive specific modulus (E_c) and specific strength (σ_c) according to ASTM D1621-16 standard. Samples had nominal dimensions of 50 × 50 × 20 mm^3, tests were carried out at 20°C and 40°C, with a crosshead speed of 2 mm/min. At least 10 specimens for each composition were tested.

The corresponding absolute values for three-point flexural and quasi-static compression tests are reported in Table S1 of the Supporting Information.

2.3.2 | Characterization of the Sandwich Composites

2.3.2.1 | Microstructural Characterization. Light microscopy was performed to assess the skin-core interfacial adhesion. The cross-section of samples was observed by using a Nikon SMZ25 optical microscope (Nikon Corporation, Tokyo, Japan).

2.3.2.2 | Mechanical Characterization. Three-point flexural tests were performed with the Instron 5969 machine (Instron Mechanical Testing Systems, Norwood, MA, USA), equipped with a load cell of 50 kN, according to the ASTM C393/C393M-20 standard. Six samples with core nominal dimensions 200 × 30 × 15 mm^3 (200 × 30 × 18 mm^3 with skins) were tested. The span length was set equal to 150 mm, and a crosshead speed of 3 mm/min was used. The tests were carried out at a constant temperature of 20°C. The test allowed us to calculate the maximum shear stress reached at the point of flexural failure (σ^{ult}_s) as expressed in Equation (6),

$$\sigma_s^{ult} = \frac{P_{max}}{(d + c) \cdot b}, \tag{6}$$

where P_{max} is the maximum load observed before failure, d is the sandwich thickness, c is the core thickness, and b is the specimen width. Moreover, the bending stress observed in the facings

at the maximum applied load, denoted as facing stress (σ_{fac}) was calculated as reported in Equation (7),

$$\sigma_{fac} = \frac{S \cdot P_{max}}{2t \cdot (d + c) \cdot b}, \quad (7)$$

where S is the span length and t the facing thickness, calculated as $(d-c)/2$.

Edgewise compression tests were performed with an Instron 5969 machine (Instron Mechanical Testing Systems, Norwood, MA, USA), equipped with a load cell of 50 kN, according to the ASTM C364/C364M-16. Six samples with core nominal dimensions $60 \times 50 \times 15\,mm^3$ ($60 \times 50 \times 18\,mm^3$ with skins) were tested. The specimens were oriented so that the uniaxial compressive load was applied parallel to the orientation of the carbon fiber in the laminate plane, therefore on a cross-sectional area of $50 \times 15\,mm^2$. The crosshead speed was fixed at 0.75 mm/min. The tests were carried out at a constant temperature of 20°C. The test allowed the calculation of the ultimate edgewise compressive strength (σ^{ult}_{ec}) as reported in Equation (8),

$$\sigma^{ult}_{ec} = \frac{P_{max}}{2t_{fs} \cdot w}, \quad (8)$$

where P_{max} is the maximum load before failure, t_{fs} is the face sheet thickness, calculated as half of the difference between the sandwich thickness and the core thickness, and w is the specimen width.

3 | Results and Discussion

3.1 | Characterization of the Foam Samples

3.1.1 | Microstructural Characterization

The microstructural characterization of the foam samples is shown in Figure 2a–d, while the distribution of cell diameter is shown in Figure 2e.

The neat EP exhibits the characteristic polyhedral, closed-cell structure characteristic of polymeric foams [32]. The corresponding magnified image shows a typical pore-wall interface with no inclusions or disruptions. When PCMs are introduced into the foam, they appear to be preferentially located in the pore walls (Figure 2b–d). When 10 wt% of PCMs is introduced into the EP foam (Figure 2b), the foam's general morphology is retained. However, as the PCM content increases from 20 wt% to 30 wt% (Figure 2c,d), the cell structure becomes less regular and the PCM particles appear more prominent within the pore walls [27]. The analysis of the cell size distribution (Figure 2e) reveals that the mean cell diameter is $342 \pm 3\,\mu m$ for neat EP and decreases by the addition of 10 wt% and 20 wt% PCM to 231 ± 85 and $269 \pm 12\,\mu m$, respectively, attributable to the nucleation effect promoted by the microcapsules [27]. However, cell diameter increases to $426 \pm 26\,\mu m$ with 30 wt% PCM content due to strut rupture and broadening effect [27]. The microstructural evolution is further supported by the data presented in Figure 3a where theoretical, apparent and bulk density values are shown, and in Figure 3b where the total, open and closed porosity values are shown.

Both the density and the porosity trends confirm the morphological modification induced by the increasing amount of PCMs. As shown in Figure 3a, the theoretical density remains almost constant, but the bulk density nearly doubles from $0.13\,g/cm^3$ of EP to $0.24\,g/cm^3$ of EP-30. The apparent density also increases particularly beyond 20 wt% of PCMs (i.e., from $0.24\,g/cm^3$ of EP to $0.30\,g/cm^3$ of EP-20 and up to $0.94\,g/cm^3$ of EP-30). This trend suggests densification of the foam structure due to incorporation of the solid filler [32]. On the other hand, as shown in Figure 3b, the total porosity of the foams decreases progressively with increasing PCM content, while the open porosity increases sharply from 47% of EP to 74% of EP-30. This is at the expense of the closed porosity, which decreases from 41% of EP to 2% of EP-30. These trends indicate a disruption in pore connectivity and a shift towards a more open-cell morphology [32]. A similar shift towards open porosity was also observed in a recent work of our group, focused on polyurethane foams containing the same PCM microcapsules [27].

3.1.2 | Thermal Characterization

Figure 4a shows the TGA thermograms and Figure 4b shows the first derivative of mass loss of the foam samples as a function of temperature. The most important results are summarized in Table 2.

According to the results of TGA tests, the PCMs undergo complete degradation before reaching 700°C whereas about 10–16 wt% final charred layer remains for all foam compositions. Generally, the incorporation of PCMs reduces the thermal stability of epoxy foam. In fact, the $T_{5\%}$ of EP decreases from 363°C to 316°C by increasing the PCM loading since PCM has an anticipated initial degradation temperature (312°C) that neat EP. On the other hand, the temperature at which the maximum degradation rate is reached (T_{max}) is approximately maintained in sample EP-10 and is slightly postponed by about 4°C–7°C in the 20 wt% and 30 wt% loaded samples compared to neat EP (406°C), due to the fact that PCMs have a higher maximum degradation temperature than EP (i.e., 436°C).

DSC thermograms of the prepared foam samples are shown in Figure 5a–c. The most important results are summarized in Table 3.

During heating, the EP sample manifests only a glass transition temperature at approximately 85°C. On the other hand, the samples containing increasing PCMs content exhibit slightly lower glass transition temperatures and endothermic peaks corresponding to the melting of the PCMs. The enthalpy of melting increases with the PCM content and reaches 36 J/g when 30 wt% of PCMs is introduced in the foam. From the melting enthalpy values, an experimental PCM weight fraction ($w_{PCM,exp}$) can be calculated as the ratio between the enthalpy of the foams and that of the neat PCMs.

These data are in good agreement with the theoretical PCM concentration, suggesting a uniform PCM distribution in the

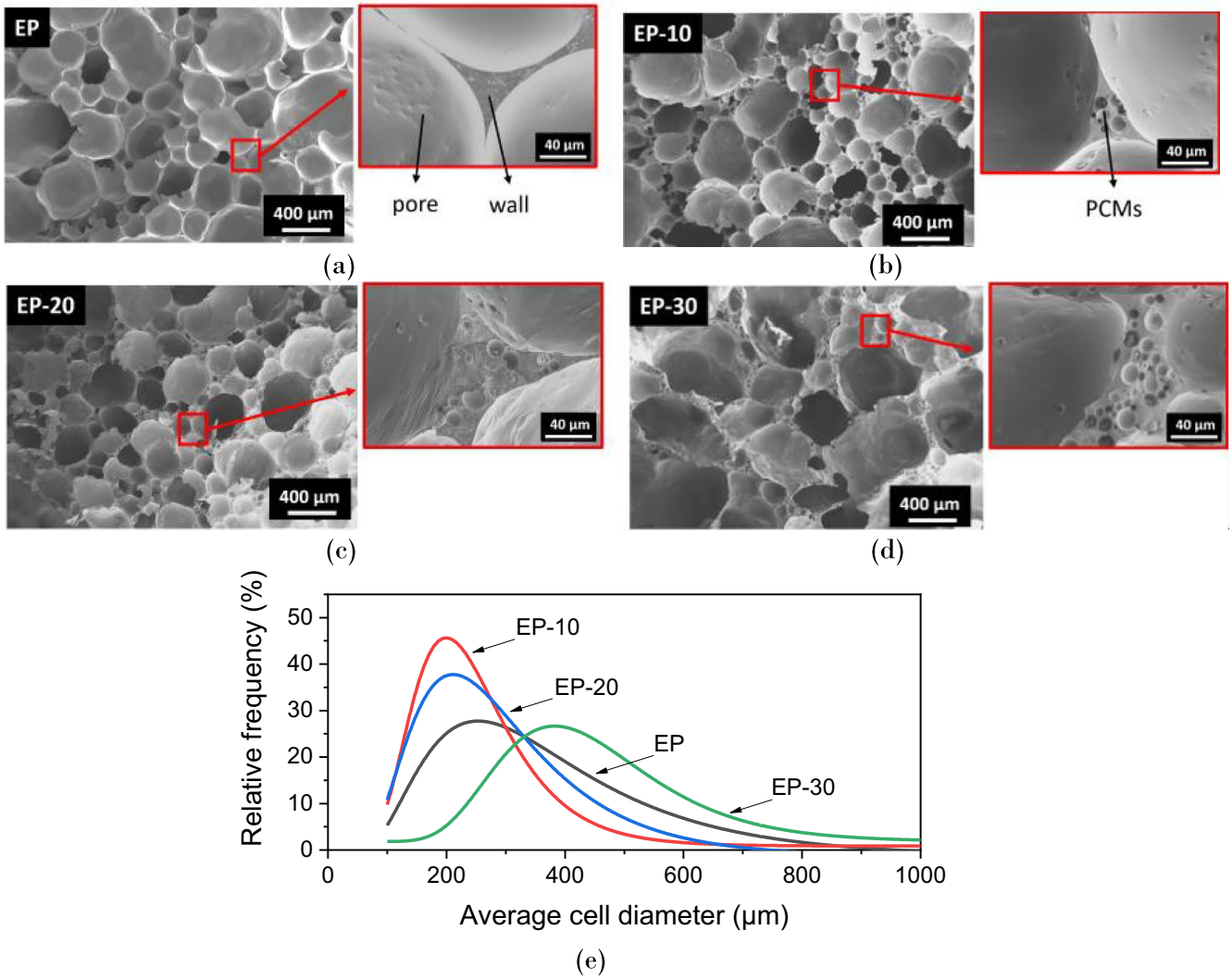

FIGURE 2 | SEM images of (a) EP, (b) EP-10, (c) EP-20 and (d) EP-30 samples. (e) Distribution of average cell diameter.

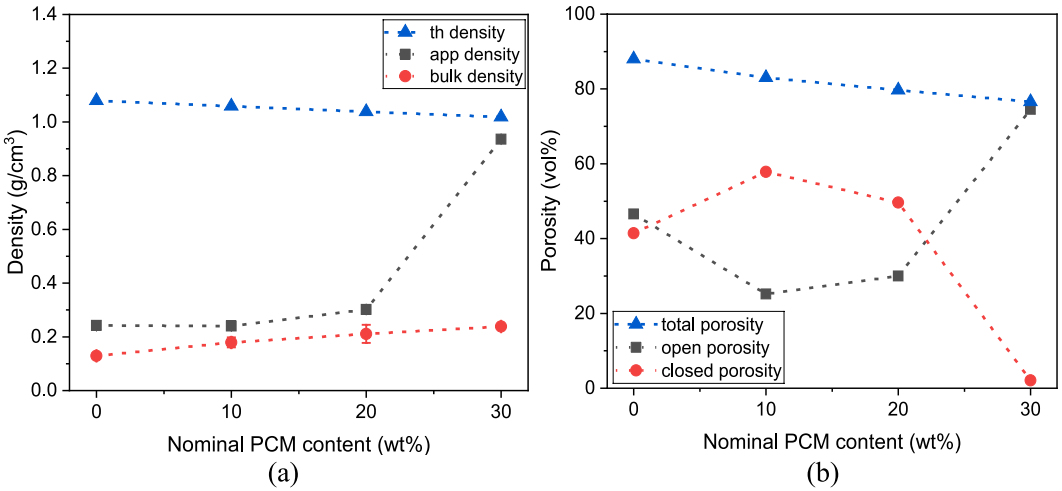

FIGURE 3 | Trends of (a) theoretical, apparent and bulk densities and (b) total, open and closed porosities.

foam and a negligible loss of PCM during sample preparation. Similar exothermic peaks are observed for the loaded samples during the cooling step (Figure 5b), which indicate the good reversibility of the phase change. During the second heating (Figure 5c), the glass transition temperature of the foams increases slightly, possibly due to some residual curing completed during the first heating [33]. The enthalpy of melting remains comparable to that observed during the first heating,

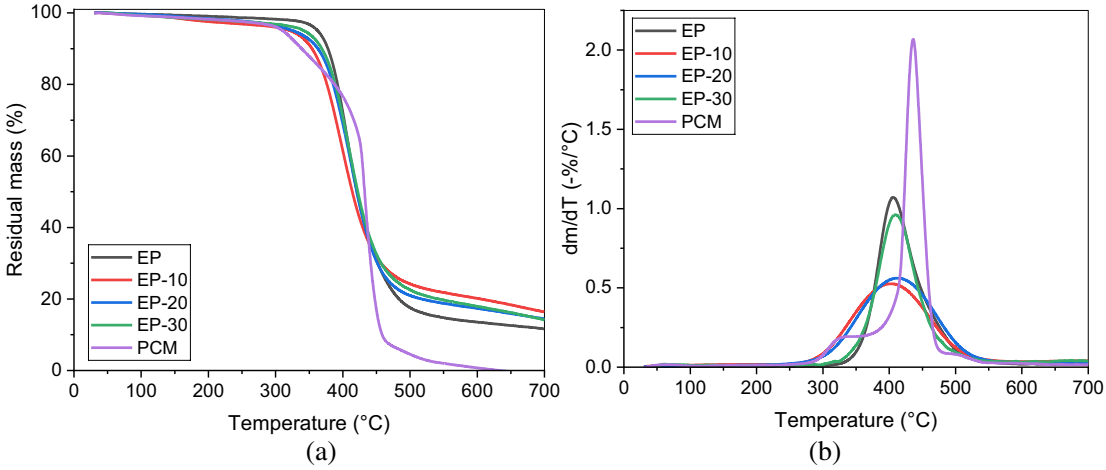

FIGURE 4 | Representative TGA thermograms of samples, (a) residual mass and (b) mass loss derivative as a function of temperature.

TABLE 2 | Results from TGA tests on the samples.

Samples	$T_{5\%}$ (°C)	T_{max} (°C)	m_{700} (%)
PCM	311.8	436.2	0
EP	363.7	406.2	11.6
EP-10	319.4	404.1	16.4
EP-20	319.2	413.3	14.5
EP-30	316.3	410.1	13.7

confirming the thermal storage capacity of the foams provided by the PCMs.

Figure 6a shows the variation in the thermal conductivity of foam samples as a function of increasing PCM content at three different testing temperatures: 10°C, 30°C and 50°C. Figure 6b shows the thermal diffusivity values from LFA analysis on the foam samples.

The thermal conductivity of EP at 10°C is 0.094 W/(m·K) and at 50°C is 0.101 W/(m·K). The increase of the PCM content up to 20 wt% does not significantly alter the thermal conductivity of the foams, which reaches a value of 0.098 W/(m·K) at 10°C and 0.106 W/(m·K) at 50°C. This trend remains consistent across all measured temperatures and it is related to the higher thermal conductivity of the PCMs compared to the EP matrix foam [34] and to the increase in open porosity observed in Figures 2c and 3b. However, the thermal conductivity shows a decrease when 30 wt% of PCMs is introduced in the foam, reaching the value of approx. 0.05 W/(m·K) for all the tested temperatures. This significant loss in thermal conductivity can be attributed to the tendency of PCM microcapsules to form aggregates at high loadings during sample preparation. These agglomerates could create heterogeneous dense regions with reduced porosity that interrupt the continuity of the foam structure and scatter the heat transfer. This interpretation is further supported by LFA analysis (Figure 6b), which shows a marked decrease in thermal diffusivity for the EP-30 sample compared to the other compositions. The drop in diffusivity indicates that heat propagation through the material becomes less efficient, possibly due to increase phonon scattering caused by the presence of PCM cluster and voids. Similar findings have been reported in other PCM–polymer systems, where a high PCM loading (30 wt%) leads to agglomeration, thus lowering the effective thermal conductivity despite the higher open porosity content [35].

In Figure 7a,b, the temperature profiles of the foam surfaces (average surface temperature) as a function of time in heating and cooling stage are reported.

The temperatures $T_{e,h}$ and $T_{e,c}$ indicate the environment temperatures during the heating (50°C) and the cooling (8°C) experiments, respectively. During the heating stage, all the samples show a general increase in temperature over time as they absorb thermal energy. EP, EP-10 and EP-20 samples reach $T_{e,h}$ after 45 min, with no substantial effect from the presence of PCMs. Instead, the effect of the PCMs is most evident at 30 wt%. Samples at this concentration exhibit a slower temperature increase and an overall lower final surface temperature (approximately 34°C) within the 45 min test period. This trend demonstrates the latent heat storage capability of the PCMs at a content of 30 wt%, which absorb thermal energy during phase transition, thereby delaying the increase in temperature on the surface of the samples. During cooling, the EP sample reaches $T_{e,c}$ in about 13 min, whereas the EP/PCM samples exhibit slower cooling rates depending on the PCM content (EP-10 in 22 min, EP-20 in 38 min and EP-30 above 45 min). This trend demonstrates the lack of thermal storage capacity in the EP foam sample, while the PCMs release heat during solidification. Figure 8a,b shows the thermography frames of the samples' surface profiles during heating and cooling at 0, 3 and 8 min, as a function of PCM concentration, as determined by previous tests.

The thermography frames confirm the thermal behavior shown previously in Figure 7a,b. During heating (Figure 8a), samples with a higher PCM content, particularly the EP-30, heat up more slowly due to their strong thermal buffering effect. During cooling (Figure 8b), the PCM-filled samples release heat more gradually than the pure EP foam. Small temperature gradients develop between the specimen borders and the core region due to heat losses at the edges. Overall, these thermography images clearly demonstrate the increased thermal inertia provided by the PCMs.

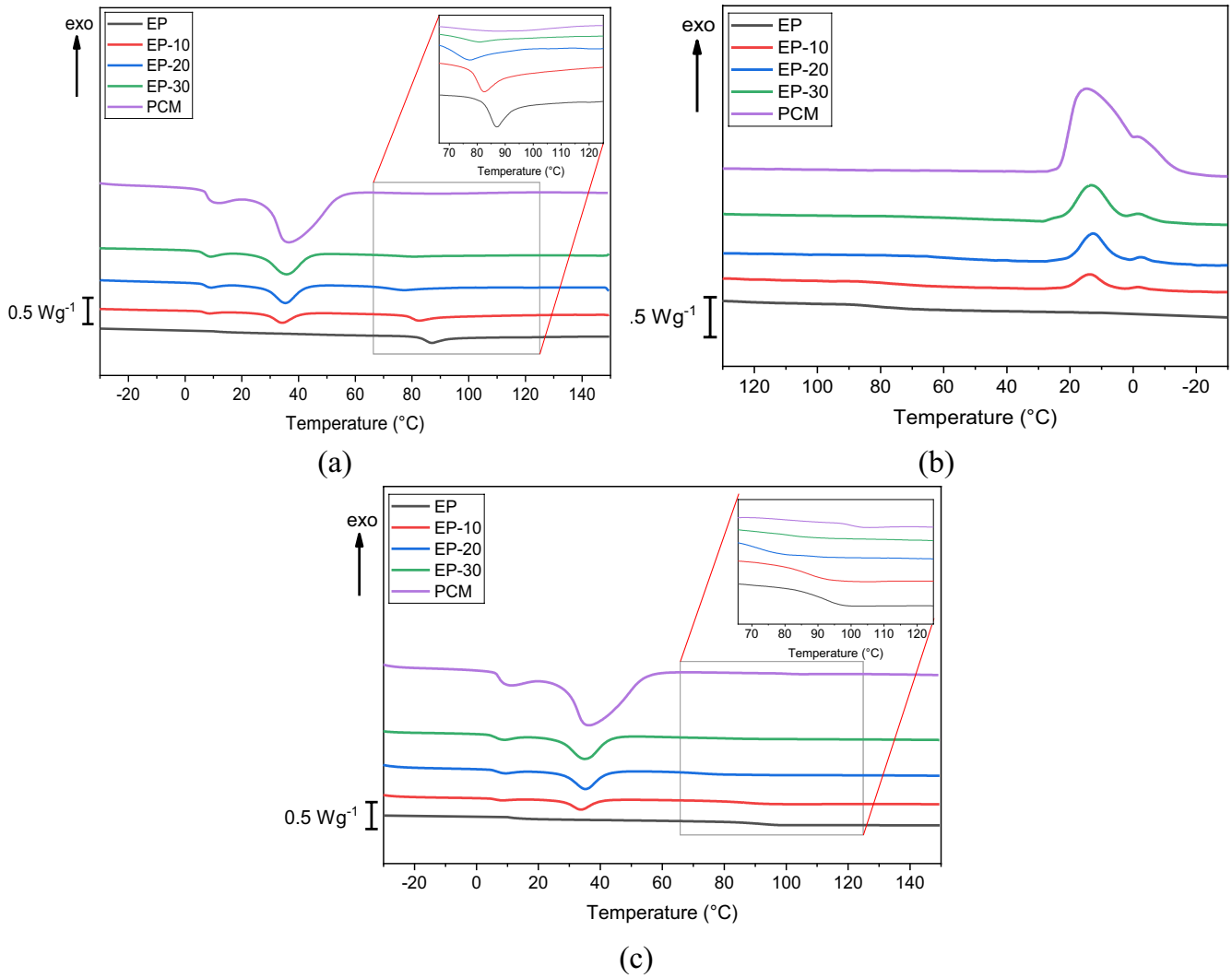

FIGURE 5 | DSC thermograms of the prepared samples, (a) first heating, (b) cooling and (c) second heating.

TABLE 3 | Results from DSC tests on the samples.

	First heating				Cooling		Second heating			
Samples	T_g (°C)	T_m (°C)	ΔH_m (J/g)	$w_{PCM,exp}$ (wt%)	ΔH_c (J/g)	T_c (°C)	T_g (°C)	T_m (°C)	ΔH_m (J/g)	$w_{PCM,exp}$ (wt%)
PCM	—	35.2	129.1	100	134.4	15.2	—	36.7	132.8	100
EP	84.8	—	—	0	—	—	84.9	—	—	0
EP-10	80.2	35.0	13.2	10.2	13.1	13.8	86.8	35.0	12.8	9.9
EP-20	72.6	34.7	27.2	21.0	25.5	13.4	73.0	34.9	25.3	19.6
EP-30	76.4	34.6	36.0	27.9	37.5	13.7	81.7	34.7	37.1	28.7

3.1.3 | Mechanical Characterization

In Figure 9a–h the representative stress–strain curves and the main results from flexural and compression tests are shown.

The introduction of PCMs generally leads to a progressive reduction in the specific mechanical properties, particularly at high loadings. Although the flexural modulus of EP (479 ± 37 MPa/(g/cm^3)) is not particularly affected by PCM content (EP-30, 437 ± 88 MPa/(g/cm^3)), the compressive modulus of EP (96 ± 32 MPa/(g/cm^3)) decreases significantly with increasing PCM content (EP-30, 35 ± 14 MPa/(g/cm^3)), indicating that the local structural modifications promoted by PCMs affect prevalently the compressive performance. The specific strengths show a similar trend, with significant reductions at 30 wt% of PCMs. In particular, the flexural strength decreases from 14 ± 1 MPa/(g/cm^3) for EP to 9 ± 3 MPa/(g/cm^3) for EP-30, and the compression strength decreases from 11 ± 1 MPa/(g/cm^3) for

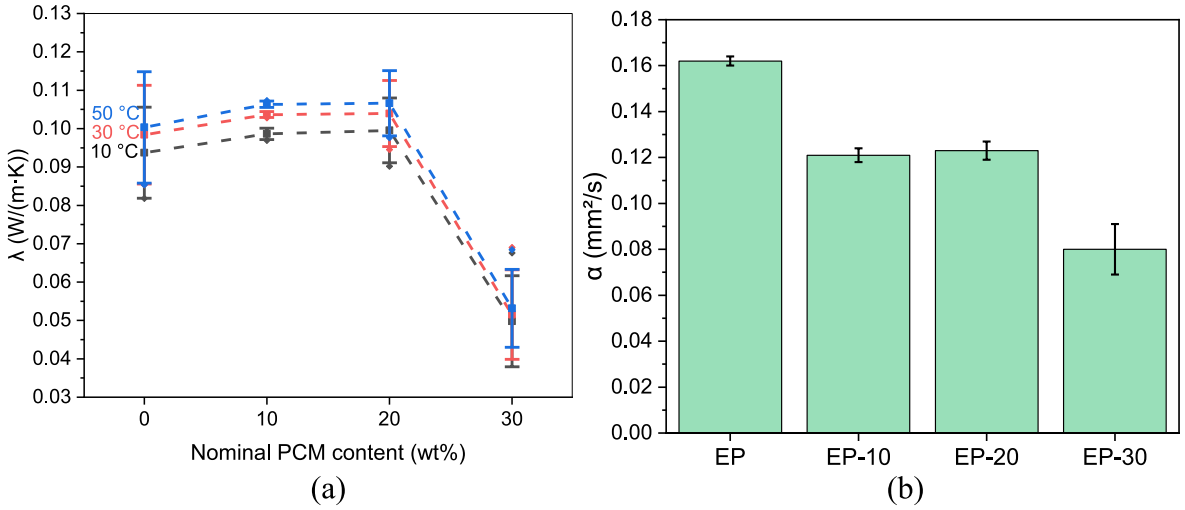

FIGURE 6 | (a) Thermal conductivity (λ) as a function of the nominal PCM concentration and the mean testing temperatures. (b) Thermal diffusivity (α) of foam samples.

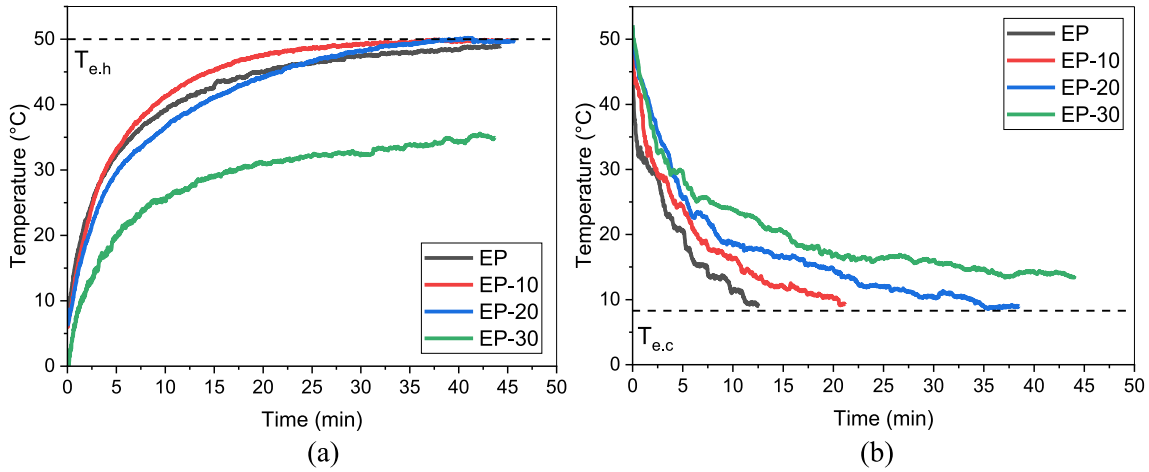

FIGURE 7 | Temperature profiles of the foam surfaces (average temperature) as a function of time during (a) heating and (b) cooling.

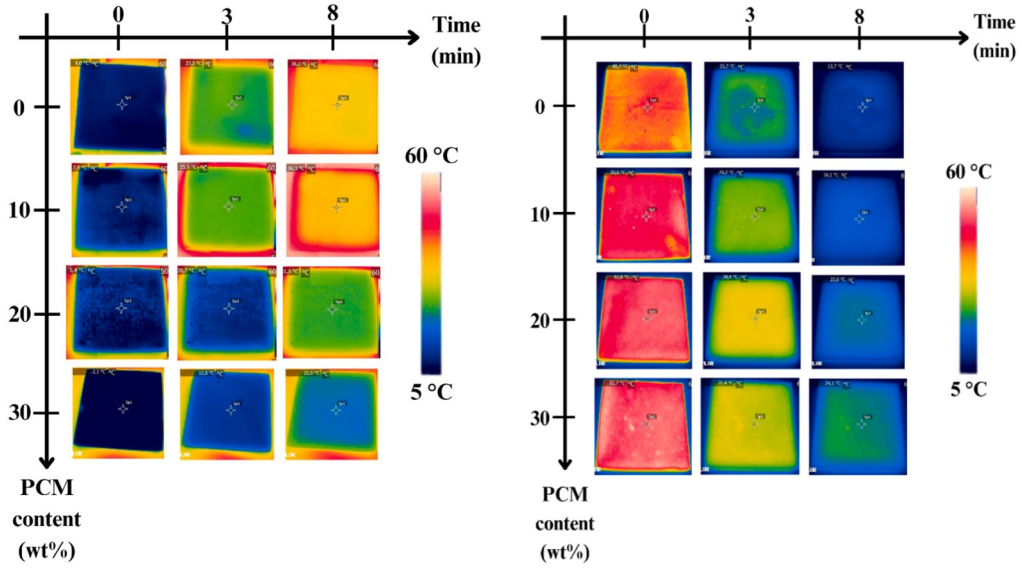

FIGURE 8 | Thermography frames at different testing time (after 0, 3, 8 min) as a function of PCM concentration during (a) heating and (b) cooling.

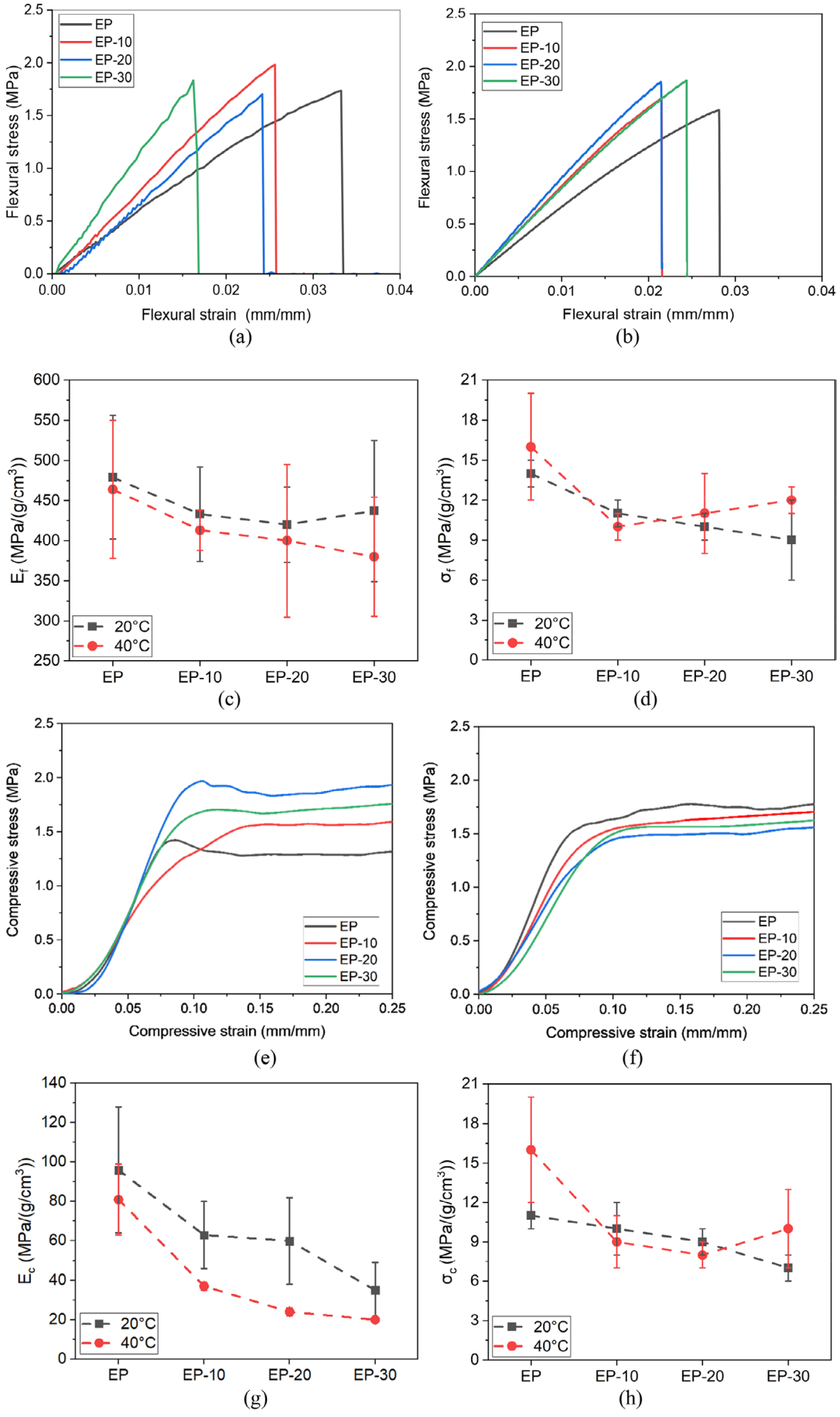

FIGURE 9 | Legend on next page.

FIGURE 9 | (a) Representative stress–strain curves of the flexural tests at 20°C and (b) at 40°C. Results of the flexural test, (c) elastic modulus and (d) flexural strength. (e) Representative stress–strain curves of the compression tests at 20°C and (f) at 40°C. Results of the compression test, (g) elastic modulus and (h) compression strength.

EP to 7 ± 1 MPa/(g/cm^3) for EP-30. As far as the influence of temperature is concerned, specific properties remain almost stable between 20°C and 40°C. This suggests that, despite the melting of the PCMs (which remain constrained within the capsule shell), the foams maintain their mechanical efficiency. Only a significant reduction in the specific compressive modulus is observed at 40°C, with values of 81 ± 18 MPa/(g/cm^3) and 20 ± 1 MPa/(g/cm^3) for EP and EP-30, respectively. Notably, the shape of the compression stress–strain curve changes significantly at 40°C, revealing that the samples exhibit no yield point at this temperature compared to 20°C. Overall, a moderate PCM content of 10–20 wt% enables satisfactory and thermally stable mechanical performance.

3.2 | Characterization of Sandwich Composites

3.2.1 | Microstructural Characterization

Light microscopy micrographs of the cross-section of the skin-core interface of samples are shown in Figure 10.

It can be observed that the laminate is firmly bonded to the foams, with no voids or defects that could affect the interfacial stability of the sandwich structure. This suggests that the application of the epoxy/hardener mixture on the foam during the hand layup process creates a strong and defect-free interface [36–39].

3.2.2 | Mechanical Characterization

Figure 11a shows the representative load–displacement curves from three-point flexural tests on the prepared sandwiches, while Figure 11b shows an image of the testing device and sample. Compressive skin failure is the predominant failure mode of samples during these kinds of tests. Figure 11c shows representative load–displacement curves from edgewise compression tests on the prepared sandwiches, and Figure 11d shows an image of the testing device and sample. Skin-core debonding is the predominant failure mode of samples during these tests.

Table 4 summarizes the most important results from three-point flexural tests and edgewise compression tests. It is worth noting that, for the sandwich mechanical tests, absolute values were deliberately considered instead of specific ones (i.e., normalized by the foam density). This choice was made because the overall mechanical response of the sandwich structures results from the combined contribution of the core, the skins and their interfacial adhesion, which are difficult to isolate and evaluate independently.

From three-point flexural tests, the load–displacement curves show that the samples fail due to an abrupt rupture, which is characteristic of skin failure in sandwich composites [40, 41]. The s-EP sample exhibits the lowest mechanical properties, with σ_s^{ult} of 0.68 MPa and σ_{fac} of 38 MPa. The incorporation of PCMs leads to an overall increase in both strength values. The s-EP-20 sample reaches improved mechanical performance, with the highest σ_s^{ult} value of 0.93 MPa (+37%) and a significant improvement in σ_{fac} to 56 MPa (+47%). On the other hand, the s-EP-10 sample exhibits improved σ_s^{ult} (0.80 MPa) and the highest σ_{fac} of 67 MPa, which correspond to a 76% increase compared to s-EP sample. However, increasing the PCM content to 30 wt% causes both the stresses to decrease to 0.76 and 45.37 MPa, respectively. This indicates a decrease in mechanical strength due to microstructural weakening induced by the excessive PCM loading. Nevertheless, these values are still higher than those of s-EP, suggesting that the presence of PCMs generally improves the mechanical performance of the structure. Therefore, data suggest that a moderate PCM content of 10–20 wt% enhances both the shear and the bending resistance of the sandwich structure, whereas excessive PCM content (above 30 wt%) could deteriorate its performance.

From edgewise compression tests, the load–displacement curves reveal an abrupt rupture, which is a failure mode indicating a strong skin-core adhesion and therefore an efficient stress transfer across the interface [42]. The s-EP sample has an edgewise compressive strength of 90 MPa, and the incorporation of PCMs results in a general increase in strength. In particular, the incorporation of 20 wt% of PCMs leads to an improvement

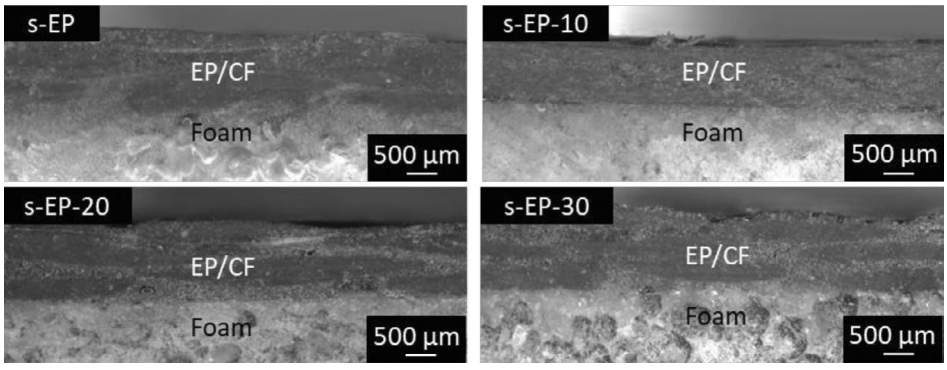

FIGURE 10 | Light microscope images of the cross-section of the sandwich samples, highlighting the skin-core interfacial adhesion.

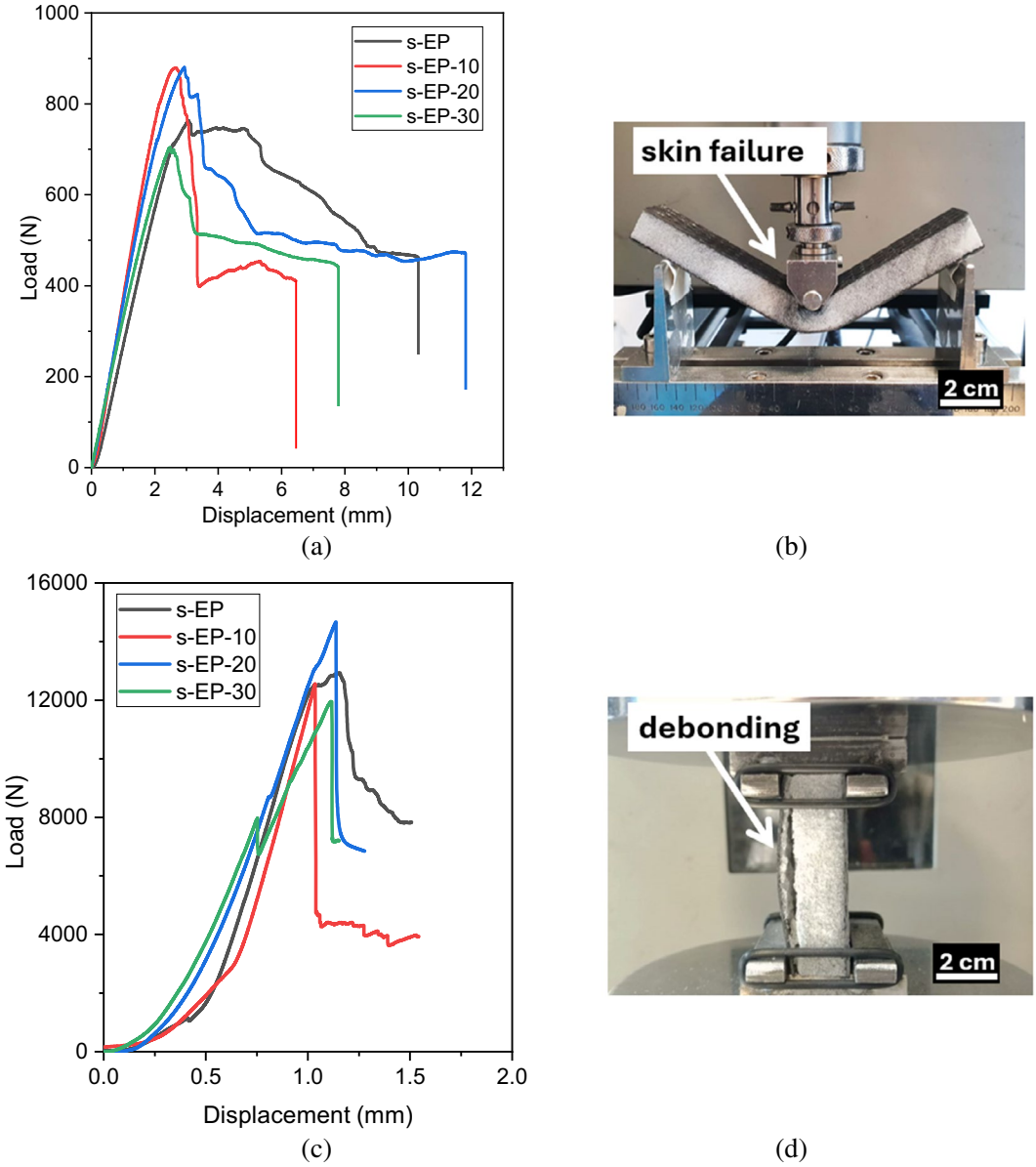

FIGURE 11 | (a) Representative load–displacement curves from three-point flexural tests on the prepared sandwiches and (b) skin failure during testing. (c) Representative load–displacement curves from edgewise compression tests on the prepared sandwiches and (d) skin-core debonding during testing.

TABLE 4 | Results of the mechanical characterization of the sandwich samples from three-point flexural tests and edgewise compression tests. In particular, the maximum shear stress (σ_s^{ult}), facing stress (σ_{fac}) and ultimate edgewise compressive strength (σ_{ec}^{ult}) are summarized.

Samples	σ_s^{ult} (MPa)	σ_{fac} (MPa)	σ_{ec}^{ult} (MPa)
s-EP	0.68 ± 0.13	38 ± 6	90 ± 38
s-EP-10	0.80 ± 0.05	67 ± 14	81 ± 24
s-EP-20	0.93 ± 0.06	56 ± 11	108 ± 19
s-EP-30	0.76 ± 0.11	45 ± 11	73 ± 29

in σ_{ec}^{ult} value up to 107.75 MPa (+20% compared to s-EP), thus indicating an improved core integrity and a better load-bearing performance of the structure. However, by increasing the PCM content up to 30 wt%, the σ_{ec}^{ult} value is reduced to 73 MPa. This decrease suggests that an excessive PCM addition weakens the foam's structure, therefore resulting in a decrease in mechanical performance. Generally, the data demonstrates that a PCM content of 20 wt% enhances the edgewise compression strength of the sandwich structure, while an excessive PCM content (30 wt%) deteriorates its performance.

4 | Conclusions

In this work, epoxy foams filled with 10%, 20% and 30% by weight of microencapsulated PCMs were developed and characterized for use as cores in sandwich composites that combine load-bearing capacity with latent heat storage. Microstructural analysis revealed that an increase in PCM content resulted in a shift from closed-cell to open-cell morphology, with the

microencapsulated material preferentially located within the cell walls. However, the incorporation of 20 wt% PCM was found not to significantly alter the original foam's morphology and porosity, while retaining good insulating properties (thermal conductivity below 0.106 W/m·K measured at 50°C). Thermal tests confirmed a progressive increase in melting enthalpy, reaching 36 J/g at 30 wt%, as well as delayed surface temperature evolution during both heating and cooling cycles achieved with 20–30 wt% PCM content. Mechanical tests showed that the flexural and compressive properties of the loaded foams generally decreased, particularly at a PCM content of 30 wt%, regardless of the testing temperature (20°C or 40°C).

When reinforced with carbon/epoxy skins, the resulting PCM-enriched sandwiches perform equally or better than those with a neat epoxy foam core. In three-point flexural tests, composites with 20 wt% PCM cores exhibited 37% greater core shear flexural strength and 47% higher facing stress than the control sample. In the edgewise compression test, the s-EP-20 sample showed an improved edgewise compressive strength of 20% compared to the control sample. Therefore, the overall results indicate that intermediate PCM contents, particularly 20 wt%, are optimal for achieving simultaneous improvement in thermal management and mechanical performance. Such multifunctional composites could play a significant role in applications where weight reduction, structural performance and thermal regulation are equally critical, including in the construction of aerospace structures, automotive components and refrigerated transport systems.

Author Contributions

Laura Simonini: conceptualization, investigation, writing – original draft, methodology, validation, visualization. **Silvia Santagiuliana:** investigation, data curation. **Alessandro Tomasini:** investigation, data curation. **Giulia Fredi:** conceptualization, writing – review and editing, validation, visualization, methodology. **Alessandro Pegoretti:** conceptualization, methodology, validation, visualization, writing – review and editing, supervision, funding acquisition.

Funding

This research activity has been supported by the Air Force Office of Scientific Research (AFOSR) within the project "Multifunctional Polymer Composites for thermal energy storage: current trends and future perspectives", Grant Number: FA8655-23–1-7039.

Acknowledgments

Open access publishing facilitated by Universita degli Studi di Trento, as part of the Wiley - CRUI-CARE agreement.

Conflicts of Interest

The authors declare no conflicts of interest.

Data Availability Statement

The data that support the findings of this study are available from the corresponding author upon reasonable request.

References

1. J. Tang, Z. Zhou, H. Chen, et al., "Laminate Design, Optimization, and Testing of an Innovative Carbon Fiber-Reinforced Composite Sandwich Panel for High-Speed Train," *Polymer Composites* 42 (2021): 5811–5829.

2. A. Kausar, I. Ahmad, S. Rakha, M. Eisa, and A. Diallo, "State-of-the-Art of Sandwich Composite Structures: Manufacturing—to—High Performance Applications," *Journal of Composites Science* 7 (2023): 102–108.

3. M. Chairi, J. El Bahaoui, I. Hanafi, et al., "Computational Assessment of Sustainable Balsa and Basalt Composite Sandwich for Structural Marine Applications," *International Journal of Damage Mechanics* 21 (2025): 1–24.

4. M. Celiński, K. Sałasińska, K. Mizera, and P. Kozikowski, "Fire Behavior of Sandwich Panels With Different Cores," *Advances in the Toxicity of Construction and Building Materials* 1 (2022): 137–170.

5. T. Zhao, J. Yang, J. Chen, and S. Guan, "Review of Carbon Fiber-Reinforced Sandwich Structures," *Polymers and Polymer Composites* 30 (2022): 789–819.

6. Y. Chen and R. Das, "A Review on Manufacture of Polymeric Foam Cores for Sandwich Structures of Complex Shape in Automotive Applications," *Journal of Sandwich Structures and Materials* 24 (2022): 789–819.

7. D. Korupolu, P. Budarapu, V. Vusa, M. Pandit, and J. C. S. J. Reddy, "Impact Analysis of Hierarchical Honeycomb Core Sandwich Structures," *Composite Structures* 280 (2022): 114827–114849.

8. F. Tarlochan, "Sandwich Structures for Energy Absorption Applications: A Review," *Materials* 14 (2021): 4731–4751.

9. D. Kwon, J. Kim, K. DeVries, and J. Park, "Optimized Epoxy Foam Interface of CFRP/Epoxy Foam/CFRP Sandwich Composites for Improving Compressive and Impact Properties," *Journal of Materials Research and Technology* 11 (2021): 62–71.

10. Y. Boztoprak, M. Ünal, Ç. Özada, et al., "Sound Insulation Performance of Honeycomb Core Aluminum Sandwich Panels With Flexible Epoxy-Based Foam Infill," *Composite Structures* 319 (2023): 117149–117163.

11. X. Wu, Y. Gao, Y. Wang, et al., "Recent Developments on Epoxy-Based Syntactic Foams for Deep Sea Exploration," *Journal of Materials Science* 56 (2021): 2037–2076.

12. G. Irven, D. Carolan, A. Fergusson, and J. P. N. Dear, "Fracture Performance of Epoxy Foam: Low Density to Bulk Polymer," *Polymer* 261 (2022): 125420–125433.

13. Z. Kamble, "Advanced Structural and Multi-Functional Sandwich Composites With Prismatic and Foam Cores: A Review," *Polymer Composites* 45 (2024): 16355–16382.

14. B. Chen, Y. Jia, F. Narita, C. Wang, and Y. Shi, "Multifunctional Cellular Sandwich Structures With Optimised Core Topologies for Improved Mechanical Properties and Energy Harvesting Performance," *Composites Part B, Engineering* 238 (2022): 109899–109911.

15. G. Fredi, A. Dorigato, L. Fambri, and A. Pegoretti, "Evaluating the Multifunctional Performance of Structural Composites for Thermal Energy Storage," *Polymers* 13 (2021): 3108–3123.

16. H. Ma, B. Gao, M. Wang, et al., "Strategies for Enhancing Thermal Conductivity of Polymer-Based Thermal Interface Materials: A Review," *Journal of Materials Science* 56 (2021): 1064–1086.

17. Z. Mahmood and U. Khan, "Unsteady Three-Dimensional Nodal Stagnation Point Flow of Polymer-Based Ternary-Hybrid Nanofluid Past a Stretching Surface With Suction and Heat Source," *Science Progress* 106 (2023): 1–26.

18. G. Soret, P. Vacca, J. Tignard, et al., "Thermal Inertia as an Integrative Parameter for Building Performance," *Journal of Building Engineering* 33 (2021): 101623–101637.

19. W. Aftab, A. Usman, J. Shi, K. Yuan, M. Qin, and R. Zou, "Phase Change Material-Integrated Latent Heat Storage Systems for Sustainable Energy Solutions," *Energy & Environmental Science* 14 (2021): 4268–4291.

20. A. Ismail, J. Wang, B. Salami, L. Oyedel, and G. Otukogbe, "Micro-encapsulated Phase Change Materials for Enhanced Thermal Energy Storage Performance in Construction Materials: A Critical Review," *Construction and Building Materials* 401 (2023): 132877–132900.

21. Z. Chang, K. Wang, X. Wu, et al., "Review on the Preparation and Performance of Paraffin-Based Phase Change Microcapsules for Heat Storage," *Journal of Energy Storage* 46 (2022): 103840–113852.

22. S. Ghani, M. Shafiqah, and S. Abidin, "Synthesis and Characterization of Stearic Acid/Waste Filler Materials as Composite Phase Change Material in Thermal Energy Storage Application," *Materials Today Communications* 107 (2024): 36–45.

23. M. Yadav, N. Pasarkar, A. Naikwadi, and P. Mahanwar, "A Review on Microencapsulation, Thermal Energy Storage Applications, Thermal Conductivity and Modification of Polymeric Phase Change Material for Thermal Energy Storage Applications," *Polymer Bulletin* 80 (2022): 5897–5927.

24. X. Zeng, S. Chen, Y. Liao, et al., "High Latent Heat and Recyclable Phase-Change Materials for Photothermoelectric Conversion," *ACS Applied Materials & Interfaces* 17 (2025): 27155–27166.

25. Y. Hu, Y. Huang, X. Liu, et al., "Synergistically Enhanced NF/CNTs@ PDA/PEG Composite Phase Change Materials for High-Efficiency Solar-Thermal Energy Storage and Conversion," *Solar Energy Materials and Solar Cells* 290 (2025): 113714.

26. H. B. Ghadim, A. Godin, A. Veillere, M. Duquesne, and D. Haillot, "Review of Thermal Management of Electronics and Phase Change Materials," *Renewable and Sustainable Energy Reviews* 208 (2025): 115039.

27. G. Fredi, E. Boso, A. Sorze, and A. Pegoretti, "Multifunctional Sandwich Composites With Optimized Phase Change Material Content for Simultaneous Structural and Thermal Performance," *Composites Part A, Applied Science and Manufacturing* 186 (2024): 108382–108400.

28. F. Galvagnini, G. Fredi, A. Dorigato, L. Fambri, and A. Pegoretti, "Mechanical Behaviour of Multifunctional Epoxy/Hollow Glass Microspheres/Paraffin Microcapsules Syntactic Foams for Thermal Management," *Polymers* 13 (2021): 2896.

29. G. Fredi, G. Ronconi, F. Galvagnini, et al., "Modeling the Thermal Behavior of Multifunctional Syntactic Foams Containing Phase Change Materials for Heat Management Applications," *Polymer Composites* 45 (2024): 15590–15603.

30. F. Galvagnini, A. Dorigato, L. Fambri, G. Fredi, and A. Pegoretti, "Thermophysical Properties of Multifunctional Syntactic Foams Containing Phase Change Microcapsules for Thermal Energy Storage," *Polymers* 13 (2021): 1790.

31. G. Fredi, "Thermal Energy Storage Composites," in *Multifunctional Structural Polymer Composites for Thermal Energy Storage and Management* (Walter de Gruyter GmbH, 2025).

32. L. Simonini, A. Sorze, L. Maddalena, F. Carosio, and A. Dorigato, "Mechanical Reprocessing of Polyurethane and Phenolic Foams to Increase the Sustainability of Thermal Insulation Materials," *Polymer Testing* 138 (2024): 108539–108553.

33. H. Shnawa, "Studies on Thermal Properties and Curing Kinetics of Talc-Filled Epoxy Resin Composite Using Differential Scanning Calorimetry," *Polymer Bulletin* 79 (2022): 11461–11478.

34. V. Skurkyte-Papieviene, A. Abraitiene, A. Sankauskaite, V. Rubeziene, and J. Baltusnikaite-Guzaitiene, "Enhancement of the Thermal Performance of the Paraffin-Based Microcapsules Intended for Textile Applications," *Polymers* 13 (2021): 1120–1136.

35. F. Galvagnini, A. Dorigato, L. Fambri, and A. Pegoretti, "Development of Novel Polypropylene Syntactic Foams Containing Paraffin Microcapsules for Thermal Energy Storage Applications," *Molecules* 27 (2022): 8520–8542.

36. L. Simonini, D. Rigotti, J. K. R. Pidapa, and A. Pegoretti, "Poly (Butylene Adipate-Co-Terephthalate) as a New Healing Agent for Epoxy/Basalt Composites," *Composites Part A, Applied Science and Manufacturing* 196 (2025): 109010–109019.

37. Y. Sun, L. Simonini, C. Xing, and L. Mishnaevsky, Jr., "Self-Healing Interfaces in Fiber Reinforced Polymers: Computational Modeling," *Composites Science and Technology* 270 (2025): 111269–111282.

38. L. Simonini and A. Dorigato, "Surface Modification of Wood Fibers With Citric Acid as a Sustainable Approach to Developing Novel Polycaprolactone-Based Composites for Packaging Applications," *Journal of Composites Science* 9 (2025): 274–289.

39. S. Pozueco, L. Simonini, H. Mahmood, et al., "Influence of CO_2 Laser Surface Treatment of Basalt Fibers on the Mechanical Properties of Epoxy/Basalt Composites," *Polymer Composites* 45 (2024): 10965–10975.

40. H. Zniker, I. Feddal, B. Ouaki, and S. Bouzakraoui, "Experimental and Numerical Investigation of Mechanical Behavior and Failure Mechanisms of PVC Foam Sandwich and GRP Laminated Composites Under Three-Point Bending Loading," *Journal of Failure Analysis and Prevention* 23 (2023): 66–78.

41. H. Junaedi, T. Khan, and T. A. Sebaey, "Characteristics of Carbon-Fiber-Reinforced Polymer Face Sheet and Glass-Fiber-Reinforced Rigid Polyurethane Foam Sandwich Structures Under Flexural and Compression Tests," *Materials* 16 (2023): 5101–5114.

42. D. S. Jebadurai and A. A. J. Kumar, "Influence of Different Core Configurations on the Skin Core Bonding of Sandwich Composites," *Journal of the Brazilian Society of Mechanical Sciences and Engineering* 45 (2023): 391–403.

Supporting Information

Additional supporting information can be found online in the Supporting Information section. **Table S1:** Comparison of absolute and specific values from the mechanical characterization of the foams tested under three-points flexural and uniaxial compression conditions.